

Article

# Numerical Investigation of Aligned Magnetic Flow Comprising Nanoliquid over a Radial Stretchable Surface with Cattaneo–Christov Heat Flux with Entropy Generation

A. Zaib <sup>1</sup>, Umair Khan <sup>2</sup> , Ilyas Khan <sup>3,\*</sup> , Asiful H. Seikh <sup>4</sup>  and El-Sayed M. Sherif <sup>4,5</sup> 

<sup>1</sup> Department of Mathematical Sciences, Federal Urdu University of Arts, Science & Technology, Gulshan-e-Iqbal, Karachi 75300, Pakistan; aurangzaib@fuuast.edu.pk

<sup>2</sup> Department of Mathematics and Social Sciences, Sukkur IBA University, Sukkur 65200, Pakistan; umairkhan@iba-suk.edu.pk

<sup>3</sup> Faculty of Mathematics and Statistics, Ton Duc Thang University, Ho Chi Minh City 72915, Vietnam

<sup>4</sup> Center of Excellence for Research in Engineering Materials (CEREM), King Saud University, P.O. Box 800, Al-Riyadh 11421, Saudi Arabia; aseikh@ksu.edu.sa

<sup>5</sup> Electrochemistry and Corrosion Laboratory, Department of Physical Chemistry, National Research Centre, El-Bethoth St. 33, Dokki, Cairo 12622, Egypt; esherif@ksu.edu.sa

\* Correspondence: ilyaskhan@tdtu.edu.vn

Received: 21 November 2019; Accepted: 13 December 2019; Published: 15 December 2019



**Abstract:** The influence of entropy generation on aligned magnetic flow-including nanoparticles through a convectively heated radial stretched surface in the existence of Cattaneo–Christov heat flux is inspected. The highly nonlinear leading PDE's via the similar scaling transformation are developed. The resulting system via the bvp4c technique from Matlab is computed. The impacts of rising constraints on the liquid velocity, nanoparticles concentration and temperature profile are argued and showed via portraits and table. In addition, the performance of liquid flow is inspected through the friction factor, the mass and heat transfer rate. With the rise in the thermal relaxation constraint, the thermal boundary layer is appreciably altered. Due to an aligned angle, the velocity of nanoliquid declines, while the concentration and temperature of nanofluid augment. It is also observed that the values of friction factor increase, whereas the values of heat and mass transfer decline due to an aligned angle. Entropy generation profiles developed due to magnetic parameters and the aligned angle. Lastly, a comparative scrutiny is composed via the previous studies which lead to support for our presently developed model.

**Keywords:** nanofluid; MHD aligned flow; convective boundary condition; entropy generation; Cattaneo–Christov heat flux

## 1. Introduction

Regular heat transport liquids similar to ethylene-glycol, water and oil have lesser thermal conductivity are characterized as poor materials and consequently cannot accomplish the lofty claim of technological and industrial fields. Modern progresses in nanotechnology permit to develop a novel group of fluids express as a nanofluid, which is initially exploited by Choi [1]. Thereafter, this topic of research has magnetized the interest of several researchers globally in light of its delightful thermal characteristics and prospective applications in several areas, for instance, biomedical, microelectronics, and transportation. Buongiorno [2] suggested the convective-transport model for nanoliquid. He scrutinized that the movement of thermophoresis and Brownian constraints of nanoparticles bestow the immense development in fluids thermal conductivity. Nield and Kuznetsov [3]

utilized the model of Buongiorno to investigate the problem of Cheng-Minkowycz for free convective flow containing nanoparticles through a vertical surface by porous media. Nanofluid towards a stretched sheet through heat transfer was considered by Khan and Pop [4]. Turkyilmazoglu [5] discussed the single model as well as multi-phase model containing nanofluids and obtained the analytic solutions. He scrutinized that the water-based Ag nanoparticle is the finest mixture of heat transfer. Pour and Nassab [6] discussed the single phase 2D laminar forced convective flow comprising nanoliquids through a backward facing step by employing bleeding conditions. Goodarzi et al. [7] utilized the model of two-phase to scrutinize the turbulent and laminar mixed convective flow of water-based copper nanoparticles through a rectangular shallow cavity. An analytical and numerical investigation on axisymmetric flow comprising nanoliquid was explored by Mustafa et al. [8]. They detected that development in Schmidt number transmits to a slimmer nanoparticles volume fraction of boundary-layer. Akbari et al. [9] discussed the laminar mixed convective flow comprising water-based water copper nanoparticle inside a micro-tube through a  $90^\circ$  angle of curvature angle by utilizing a finite volume technique. The unsteady flow of a Carreau fluid containing nanofluids over a stretched surface was scrutinized by Khan and Azam [10]. They explored that Nusselt number as well as Sherwood number are deflating due to thermophoresis parameter. Hussanan et al. [11] investigated the characteristics of inertial and microstructure containing magnetic ferrofluid towards a stretching/shrinking surface via an efficient model of thermal conductivity with a suction/injection. They scrutinized that a notable modification happens to the micro rotation velocity due to suction/injection. Rafique et al. [12] examined the impacts of Dufour and Soret numbers on magneto flow comprising nanoliquid through an inclined non-linear radiative surface with micropolar fluid. They showed that the velocity declines due to the nonlinear stretchable factor. Yousefzadeh et al. [13] studied the laminar flow through an open cavity by taking three distinct areas of heat transfer with mixed convection and different geometries. Faraz et al. [14] discussed the magnetic impact on time dependent flow involving Casson nanofluid through a radially stretched surface with mixed convection. Bagherzadeh et al. [15] investigated the laminar magneto flow of water based  $Al_2O_3$  nanoparticle through a rectangular micro-channel with slip condition. They observed that the magnetic force squeezes the liquid to the bottom wall. Recently, Tian et al. [16] examined the impact of different surfactants on sediment of surface and coefficient of pool boiling heat transfer of water-based DI/silica nanoparticles and obtained the results experimentally.

Entropy generation which has been utilized to measure the importance of irreversibility connected to friction, heat transport and additional non-ideal processes in a thermal system. To enhance the presentation of any heat transport procedure, entropy generation has been widely used as a useful tool. Spasojević et al. [17] used minimization of entropy generation in column of diabetic refinement through trays, where they considered the exchanged heat as a control variable rather than temperature. Abu-Nada [18] scrutinized the influence of suction/injection about a backward facing step below bleeding conditions with entropy generation. Finite volume technique is utilized to obtain the solution of leading equations. Entropy generation under the impact of magnetic field over an inclined permeable planar channel was scrutinized by Komurgoz et al. [19]. They noticed that the highest entropy generation was acquired in the absence of porosity and magnetic parameters. Further, Butt and Ali [20] explored the influences of thermal radiation and entropy generation on hydro magnetic free convective flow towards a vertical surface entrenched in permeable media. Rashidi et al. [21] examined the entropy generation on magneto flow towards a rotated disk entrenched in a permeable medium through slip impact and variable properties. Goodarzi et al. [22] scrutinized the impact of thermal radiation on turbulent and laminar mixed convective flow through an enclosure by semitransparent medium with entropy generation. The time dependent magneto flow of four water-based nanoparticles (Cu, Ag,  $Al_2O_3$  and  $TiO_2$ ) through an accelerating stretched sheet with the convective boundary condition and entropy generation was discussed by Das et al. [23]. Shateyi et al. [24] used a relaxation spectral technique to inspect the entropy generation on magneto flow involving Maxwell liquid from a stretched surface. The influence of entropy generation using two significant slip mechanisms of

Jeffery fluid including nanofluid was examined by Rehman et al. [25]. Almakki et al. [26] explored the impact of unsteady MHD axisymmetric flow of a nanoliquid towards a nonlinear stretched surface with entropy generation. The minimization of entropy generation on magneto flow induced by the slandering stretched surface with Joule and frictional heating was scrutinized by Afridi et al. [27]. Hayat et al. [28] discussed the importance of entropy generation on flow through a stretched surface with mixed convection, non-linear heat flux and source/sink. Aghaei et al. [29] examined the entropy generation of a water based multi wall carbon nanotube with vertical as well as horizontal baffles inside an enclosure with mixed convection. El-Aziz and Afify [30] explored the influence of Hall current on the magneto flow of Casson liquid from a stretched sheet with slip effect and entropy generation. They found that entropy generation is increased due to magnetic number and decreased due to slip, Casson parameter, Eckert number, and Hall parameter. Recently, Pordanjani et al. [31] scrutinized the combined impacts of thermal radiation and magnetic field on free convective flow comprising nanofluid inside a cavity with entropy generation. They observed that the heat transfer along with entropy generation decline due to angle of magnetic parameter.

In heat conduction, the Fourier's model is very significant for the mechanism of heat transfer. For the increment of heat transfer, a thermal time relaxation in Fourier's law was suggested by Cattaneo [32]. However, several thermal relaxation times have dissimilar materials. Taking into account, Christov [33] modified a time derivative known as a model of Cattaneo–Christov heat flux which is extremely important for analysis of convective heat transfer. Straughan [34] discussed the importance of Cattaneo–Christov heat flux on Newtonian incompressible liquids with downward gravity. He examined that effect of thermal relaxation significantly increased due to Cattaneo number. Li et al. [35] considered the Cattaneo–Christov model of heat flux on viscoelastic fluid over a vertical stretched surface with magnetic field and partial slip. The impact of homogenous-heterogeneous on magneto flow involving third grade fluid with Cattaneo–Christov with the convective boundary condition was scrutinized by Ramzan et al. [36]. Hashim and Khan [37] examined the homogenous-heterogeneous influence on flow involving Carreau liquid from a slandering stretched sheet with Cattaneo–Christov effect. They observed that temperature of fluid is lower in case of Cattaneo–Christov model compared to Fourier's heat model. After the fundamental work of Christov, many researchers recently were attempted in this perspective are presented in the [38–41].

The literature discussed above exposes that the impact of aligned magnetic field along with Cattaneo–Christov heat flux comprising nanofluid from a radial stretched surface is not yet considered. Therefore, in this research, the influence of aligned magnetic flow containing nanoparticles through a convectively heated radial stretched sheet with Cattaneo–Christov heat flux is discussed. This assessment added a narrative approach for researchers and scientists to scrutinize the characteristics of nanofluid along with characteristics of heat and mass transfer. Similarity equations are built and acquired the computational solution via the bvp4c solver. The impacts of the significant restrictions are discussed in detail through graphs and table. The present analysis explains the significant features in the skin burns, heat propagation in tissues, laser surgery in biomedical engineering and food technology.

## 2. Problem Formulation

A steady magnetic aligned flow towards a radial stretched surface comprising nanoparticles is scrutinized. The surface is stretchable in the radially way with velocity  $\ddot{u}_w(\ddot{r}) = c\ddot{r}$ , where  $c$  is invariable along with an aligned acute angle  $\zeta$  is pertained. Heat flux has been characterized via the theory of Cattaneo–Christov. The lower surface is further supposed to be convectively heated from hot liquid at  $\ddot{T}_f$ , which presents a transfer of heat coefficient  $\ddot{h}_f$ . The leading relevant equations through these postulations are as engraved

$$\frac{\partial \ddot{w}}{\partial \ddot{z}} = -\frac{\ddot{u}}{\ddot{r}} - \frac{\partial \ddot{u}}{\partial \ddot{r}} \quad (1)$$

$$\ddot{w} \frac{\partial \ddot{u}}{\partial \ddot{z}} + \ddot{u} \frac{\partial \ddot{u}}{\partial \ddot{r}} = \ddot{v} \frac{\partial^2 \ddot{u}}{\partial \ddot{z}^2} - \frac{\sigma \ddot{B}_0^2}{\dot{\rho}} \ddot{u} \sin^2 \zeta \tag{2}$$

$$\ddot{w} \frac{\partial \ddot{T}}{\partial \ddot{z}} + \ddot{u} \frac{\partial \ddot{T}}{\partial \ddot{r}} - \ddot{\alpha} \frac{\partial^2 \ddot{T}}{\partial \ddot{z}^2} = \Omega \left[ \left( \frac{\ddot{D}_T}{\ddot{T}_\infty} \right) \left( \frac{\partial \ddot{T}}{\partial \ddot{z}} \right)^2 + \ddot{D}_B \frac{\partial \ddot{C}}{\partial \ddot{z}} \frac{\partial \ddot{T}}{\partial \ddot{z}} \right] - \Gamma \left[ \ddot{u}^2 \frac{\partial^2 \ddot{T}}{\partial \ddot{r}^2} + \ddot{w}^2 \frac{\partial^2 \ddot{T}}{\partial \ddot{z}^2} + 2\ddot{u}\ddot{w} \frac{\partial^2 \ddot{T}}{\partial \ddot{r}\partial \ddot{z}} + \ddot{u} \frac{\partial \ddot{u}}{\partial \ddot{r}} \frac{\partial \ddot{T}}{\partial \ddot{r}} + \ddot{w} \frac{\partial \ddot{u}}{\partial \ddot{z}} \frac{\partial \ddot{T}}{\partial \ddot{r}} + \ddot{u} \frac{\partial \ddot{w}}{\partial \ddot{r}} \frac{\partial \ddot{T}}{\partial \ddot{z}} + \ddot{w} \frac{\partial \ddot{w}}{\partial \ddot{z}} \frac{\partial \ddot{T}}{\partial \ddot{z}} \right] \tag{3}$$

$$\ddot{u} \frac{\partial \ddot{C}}{\partial \ddot{r}} - \ddot{D}_B \frac{\partial^2 \ddot{C}}{\partial \ddot{z}^2} + \ddot{w} \frac{\partial \ddot{C}}{\partial \ddot{z}} = \left( \frac{\ddot{D}_T}{\ddot{T}_\infty} \right) \left( \frac{\partial^2 \ddot{T}}{\partial \ddot{z}^2} \right) \tag{4}$$

The physical boundary conditions are

$$\begin{aligned} \ddot{w} = 0, \ddot{u} - \ddot{u}_w(\ddot{r}) = 0, \ddot{C} - \ddot{C}_w = 0, k \frac{\partial \ddot{T}}{\partial \ddot{z}} + \ddot{h}_f(\ddot{T}_f - \ddot{T}) = 0 \text{ at } \ddot{z} = 0, \\ \ddot{C} - \ddot{C}_\infty \rightarrow 0, \ddot{u} \rightarrow 0, \ddot{T} - \ddot{T}_\infty \rightarrow 0 \text{ as } \ddot{z} \rightarrow \infty. \end{aligned} \tag{5}$$

where  $(\ddot{w}, \ddot{u})$  are elements of velocity in  $\ddot{z}$ -,  $\ddot{r}$ - directions, respectively,  $\ddot{v}$  the kinematic viscosity,  $\dot{\rho}$  the density,  $\ddot{\sigma}$  the electrical conductivity,  $\ddot{\alpha}$  the thermal diffusivity,  $\ddot{B}_0$  the strength of magnetic field,  $\ddot{T}$  the temperature,  $\Gamma$  time relaxation of heat flux,  $\ddot{C}$  concentration of nanoparticles,  $\ddot{D}_T$  the thermophoresis diffusion and  $\ddot{D}_B$  the Brownian constraint,  $k$  the coefficient of thermal conductivity, and  $\Omega$  is the ratio  $b/w$  the effective heat-capacity of the substance of nanoparticles and specific heat-capacity of the fluid.

The similarity transformation is used as:

$$\ddot{u} = c\ddot{r}f'(\eta), \ddot{w} = -2\sqrt{c\ddot{v}}f(\eta), \eta - \ddot{z} \sqrt{\frac{c}{\ddot{v}}} = 0, \phi(\eta) - \frac{\ddot{C} - \ddot{C}_\infty}{\ddot{C}_w - \ddot{C}_\infty} = 0, \theta(\eta) - \frac{\ddot{T} - \ddot{T}_\infty}{\ddot{T}_f - \ddot{T}_\infty} = 0. \tag{6}$$

In light of this relation (6), Equations (2)–(4) are transmuted to

$$f''' - f'^2 + 2ff'' - M^2 f' \sin^2 \zeta = 0 \tag{7}$$

$$\theta'' + 2Prf\theta' + PrNb\theta'\phi' + PrNt\theta'^2 - Pr\tau(f^2\theta'' + ff'\theta') = 0 \tag{8}$$

$$\phi'' + 2Scf\phi' + \frac{Nt}{Nb}\theta'' = 0 \tag{9}$$

The converted boundary restrictions are

$$\left. \begin{aligned} f(0) = 0, f'(0) - 1 = 0, \theta'(0) + \gamma(1 - \theta(0)) = 0, \phi(0) = 1, \\ f'(\infty) \rightarrow 0, \theta(\infty) \rightarrow 0, \phi(\infty) \rightarrow 0. \end{aligned} \right\} \tag{10}$$

where ' points out the differentiation to  $\eta$ , magnetic parameter, Brownian parameter, thermal relaxation parameter, thermophoresis parameter, Prandtl number, convective parameter, the Schmidt number.

$$\begin{aligned} M = \sigma \ddot{B}_0^2 / c\dot{\rho}, Nb = -\ddot{D}_B \Omega (\ddot{C}_\infty - \ddot{C}_w) / \ddot{v}, \tau = 4\Gamma c, \\ Nt = -\ddot{D}_T \Omega (\ddot{T}_\infty - \ddot{T}_f) / \ddot{T}_\infty \ddot{v}, Pr = \ddot{v} / \ddot{\alpha}, \gamma = \ddot{h}_f \sqrt{\ddot{v} / c} / k, Sc = \ddot{v} / \ddot{D}_B \end{aligned}$$

The significant physical quantities which are well-defined as

$$C_{fr} = \frac{\tilde{\tau}_w}{\rho \ddot{u}_w^2}, Nu_r = -\frac{\ddot{r}q_w}{k(\ddot{T}_f - \ddot{T}_\infty)}, Sh_r = \frac{-\ddot{r}m_w}{\ddot{D}_B(\ddot{C}_\infty - \ddot{C}_w)}, \tag{11}$$

where  $\tilde{\tau}_w$ ,  $q_w$ ,  $m_w$  the shear stress, the heat and mass flux, respectively are described as

$$\tilde{\tau}_w = \mu \left( \frac{\partial \ddot{u}}{\partial \ddot{z}} \right)_{\ddot{z}=0}, \quad q_w = -k \left( \frac{\partial \ddot{T}}{\partial \ddot{z}} \right)_{\ddot{z}=0}, \quad m_w = -\ddot{D}_B \left( \frac{\partial \ddot{C}}{\partial \ddot{z}} \right)_{\ddot{z}=0} \quad (12)$$

That is,

$$C_{f_r} \text{Re}_r^{1/2} = f''(0), \quad Nu_r \text{Re}_r^{-1/2} = -\theta'(0), \quad Sh_r \text{Re}_r^{-1/2} = -\phi'(0). \quad (13)$$

where  $\text{Re}_r = \frac{\ddot{u}_w}{\ddot{\nu}}$  is the local Reynolds number.

### 3. Analysis of Entropy Generation

Entropy generation in the existence of MHD aligned flow containing nanofluid is engraved as

$$S_{gen}''' = \frac{\mu}{\ddot{T}_\infty} \left( \frac{\partial \ddot{u}}{\partial \ddot{z}} \right)^2 + \frac{k}{\ddot{T}_\infty^2} \left( \frac{\partial \ddot{T}}{\partial \ddot{z}} \right)^2 + \frac{\sigma \ddot{B}_0^2}{\ddot{T}_\infty} \ddot{u}^2 \sin^2 \zeta + \frac{RD}{\ddot{T}_\infty} \left( \frac{\partial \ddot{T}}{\partial \ddot{z}} \right) \left( \frac{\partial \ddot{C}}{\partial \ddot{z}} \right) + \frac{RD}{\ddot{C}_\infty} \left( \frac{\partial \ddot{C}}{\partial \ddot{z}} \right)^2 \quad (14)$$

The entropy generation volumetric has two factors, (i) Irreversibility (HTI) of heat transport and (ii) Irreversibility (FFI) of liquid friction (iii) Diffusive Irreversibility. It is considered as

$$S_0''' = \frac{k(\Delta \ddot{T})^2}{L^2 \ddot{T}_\infty^2} \quad (15)$$

in dimensionless form

$$N_G = \frac{S_{gen}'''}{S_0'''} = \frac{\text{Re}_L Br}{\Omega_1} f''^2 + \text{Re}_L \theta'^2 + \frac{\text{Re}_L Br}{\Omega_1} M^2 f'^2 \sin^2 \zeta + \text{Re}_L \lambda \left( \frac{\delta}{\Omega_1} \right)^2 \phi'^2 + \text{Re}_L \lambda \left( \frac{\delta}{\Omega_1} \right) \theta' \phi' \quad (16)$$

where  $\Omega_1 = \Delta \ddot{T} / \ddot{T}_\infty$ ,  $Br = \mu \ddot{u}_w^2 / k \Delta \ddot{T}$ ,  $\text{Re}_L = c L^2 / \ddot{\nu}$ ,  $\delta = \Delta \ddot{C} / \ddot{C}_\infty$ ,  $\lambda = RD \ddot{C}_\infty / k$ , the difference of temperature, the Brinkman number, the characteristic length based Reynolds number, the difference of concentration and the diffusive constant parameter, respectively. To check whether the entropy generation through dominates of heat transfer by entropy generation due to the liquid friction, the magnetic field and the diffusive irreversibility, or vice versa. The Bejan number is described

$$Be = \frac{\tilde{N}_1}{N_G} = \frac{1}{1 + \Phi} \quad (17)$$

where  $\tilde{N}_1 = \text{Re}_L \theta'^2$ . Undoubtedly, the range of Bejan number is between 0 and 1 ( $0 \leq Be \leq 1$ ). If  $Be = 0$ , then irreversibility is governed through liquid friction. If  $Be = 1$ , then irreversibility is governed through heat transfer and if  $Be = 0.5$ , this implies that the irreversibility of heat transfer and friction are the identical.

### 4. Results and Discussion

The transmuted nonlinear ODE's (7)–(9) through the converted boundary restrictions (10) are deciphered numerically via the `bvp4c` solver. The influences of relevant constraints concerning in the liquid flow problem are argued via tables and graphs. The range of the physical parameters are considered as  $0 \leq \zeta \leq \pi/2$ ,  $0 \leq M \leq 3$ ,  $0 \leq \tau \leq 1.4$ ,  $0.1 \leq Nb \leq 1$ ,  $0.1 \leq Nt \leq 1.2$ ,  $0.3 \leq \gamma \leq 0.8$ ,  $0.5 \leq Sc \leq 1$ ,  $1 \leq Pr \leq 6.2$ ,  $0.5 \leq \text{Re}_L \leq 2$ ,  $0.5 \leq Br \leq 2$ ,  $0.01 \leq \Omega \leq 0.2$ ,  $0.005 \leq \lambda \leq 0.01$ . Table 1 presents the evaluation of the current results of  $f''(0)$  with the results of Butt and Ali [42] and Soid et al. [43] in

restrictive cases are closely harmonized, which guaranteed the soundness of the present methodology. Geometry of the problem is given in Figure 1.

**Table 1.** Comparison of  $f''(0)$  for different  $M^2$  when  $\chi = 0$ ,  $\zeta = \pi/2$ .

$M^2$	Butt and Ali [42]	Mathematical Error	Soid et al. [43]	Mathematical Error	Present
0	-1.17372	0.00002	-1.17372088	0.00002088	-1.1737
0.5	-1.36581	0.00001	-1.36581449	0.00001449	-1.3658
1	-1.53571	0.00001	-1.53571052	0.00001052	-1.5357
2	-1.83049	0.00001	-1.83048967	0.00001033	-1.8305
3	-2.08484	0.00004	-2.08484656	0.00004656	-2.0848

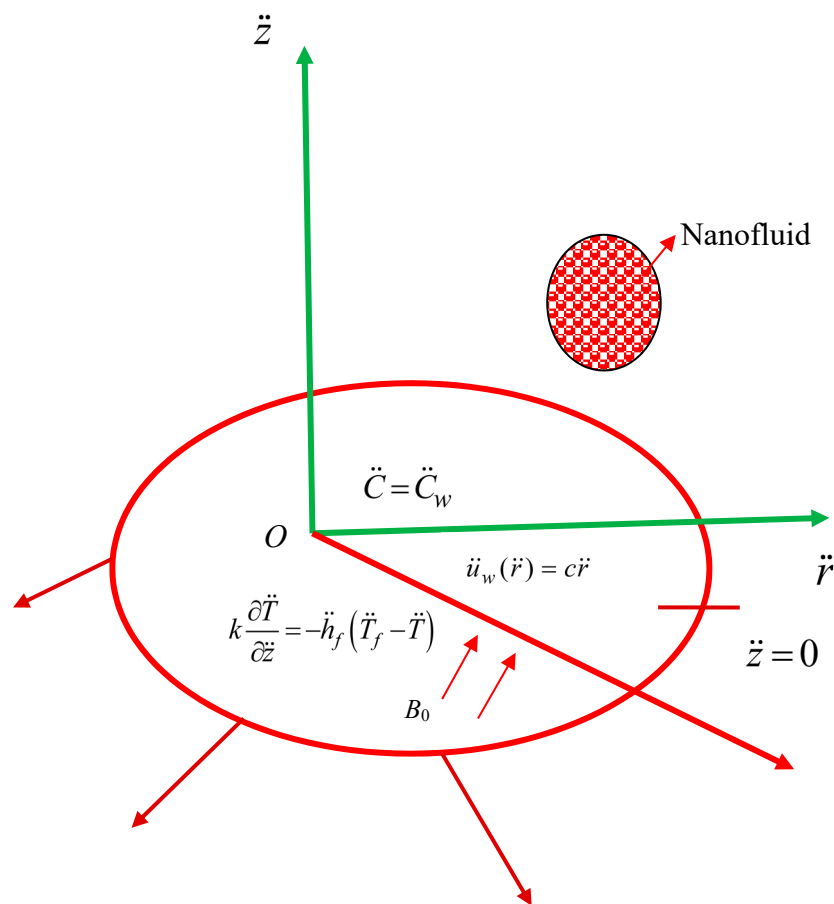


**Figure 1.** Physical diagram and coordinate system.

Figures 2–4 scrutinize the impact of aligned angle  $\zeta$  on  $f'(\eta)$ ,  $\theta(\eta)$  and  $\phi(\eta)$ . Figure 2 elucidates that the momentum boundary layer showing a decelerating behavior for the velocity profile with boost up the parameter  $\zeta$ . Since the impact of larger values of aligned angle builds a stronger impression on the external magnetic field. Despite this, the thermal and concentration boundary layers in both profiles signify an enhancing behavior as depicted in Figures 3 and 4, respectively.

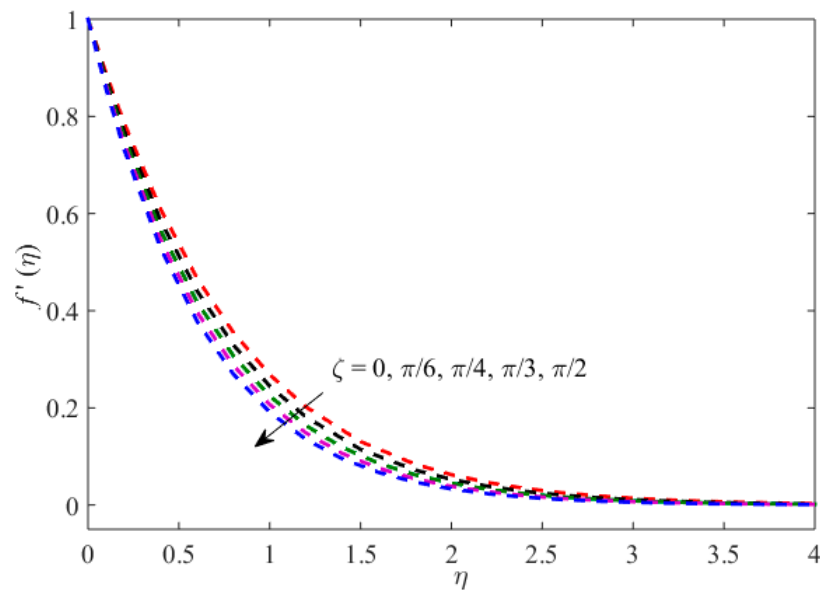


Figure 2. The influence of  $\zeta$  on  $f'(\eta)$ .

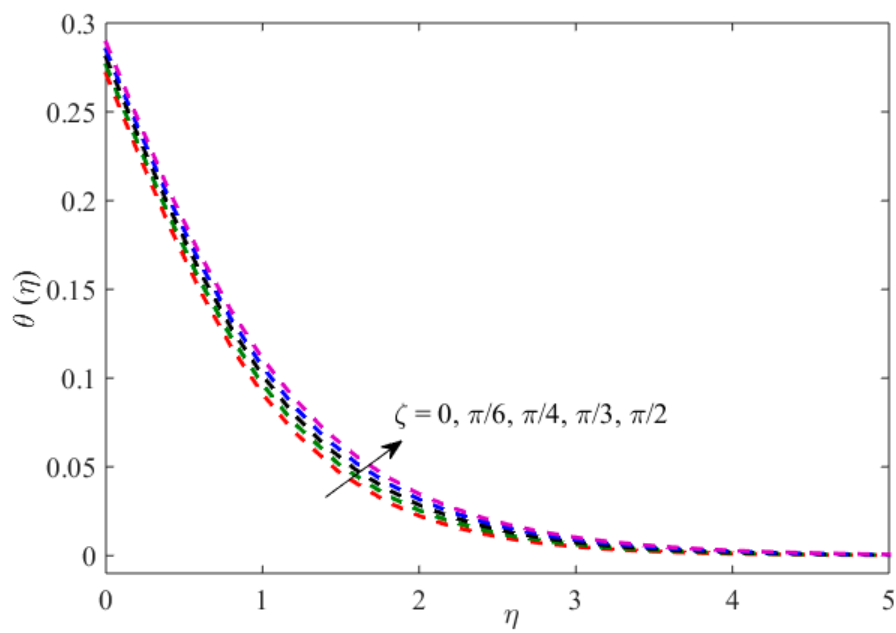
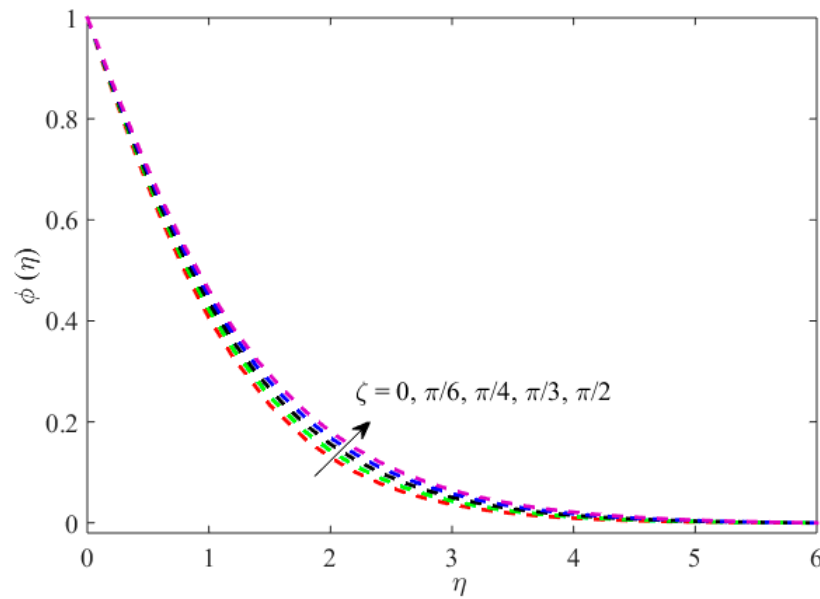
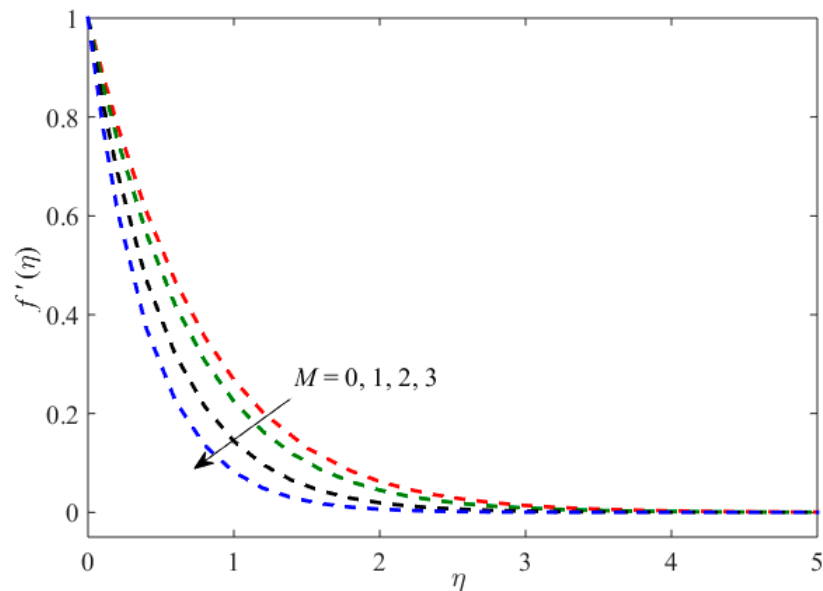


Figure 3. The influence of  $\zeta$  on  $\theta(\eta)$ .



**Figure 4.** The influence of  $\zeta$  on  $\phi(\eta)$ .

Figures 5–7 highlight the influence of magnetic field on  $f'(\eta)$ ,  $\theta(\eta)$  and the volume fraction of nanoparticles. Figure 5 scrutinize that the fluid velocity shows a downtrend due to swelling values of  $M$ . Since the magnetic constraint is communicated with a resistive drag type force (Lorentz force), so enhance in  $M$ , which offers an extra friction to the fluid flow which in turn diminishes the velocity. Figures 6 and 7 explain that the concentration and thermal boundary layers growing higher and higher in both profiles as  $M$  enhances. Physically, the Lorentz strength gives a supplementary confrontation to the flow of fluid particle. Thus, more temperature is generated which consequently escalates the temperature distribution.



**Figure 5.** The influence of  $M$  on  $f'(\eta)$ .

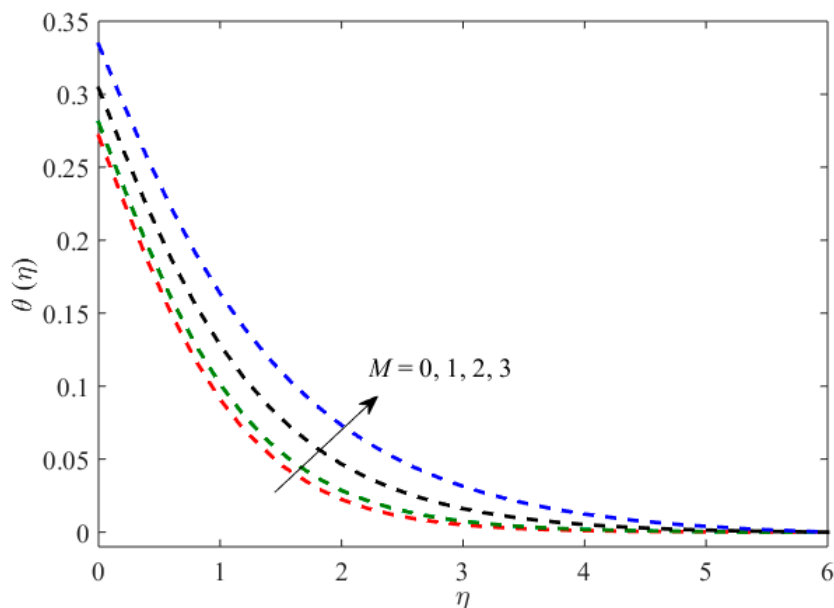


Figure 6. The influence of  $M$  on  $\theta(\eta)$ .

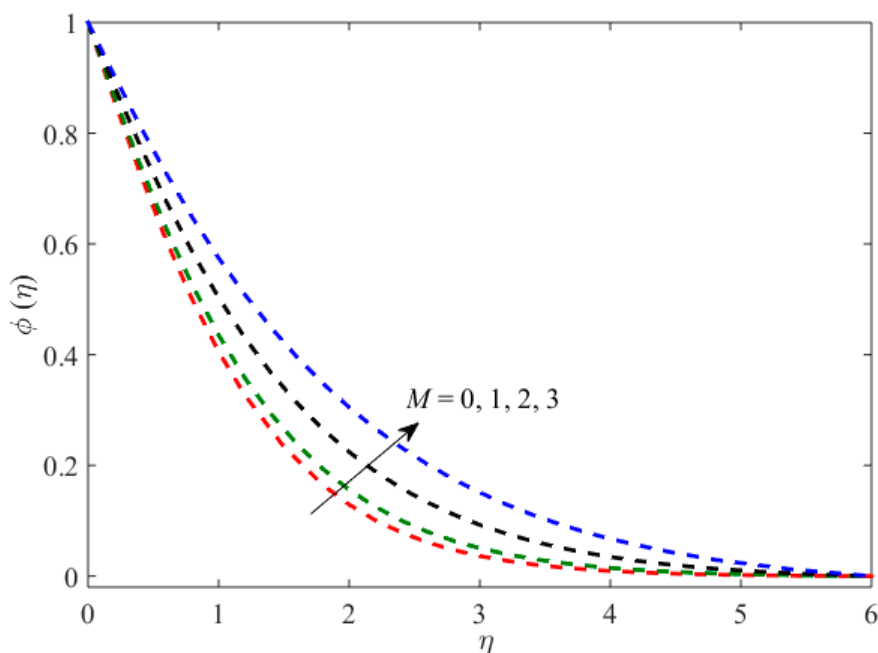


Figure 7. The influence of  $M$  on  $\phi(\eta)$ .

Figures 8 and 9 are set to monitor the motion of Brownian  $Nb$  and thermophoresis parameter  $Nt$  on the distribution of temperature profile and nanoparticles concentration profile. The thermal boundary layer mounting for the temperature distribution as we augmented the values of  $Nb$  and graphically behavior is captured in Figure 8. Physically, the nanoparticles kinetic energy enhances owing to the strength of the chaotic motion and thus, the fluid temperature raises. It is inspected from Figure 8 that the nanoparticles concentration decays because of enhancing  $Nb$ . Therefore, the motion of Brownian parameter builds the warm liquid inside the boundary and intensifies particle deposition left from the fluid regime to sheet at that time that causing in a decline in nanoparticles concentration and the thickness of the boundary-layer. The higher Brownian motion values involve the strong performance for the minor particle, while the lesser values of  $Nb$  pertained for stronger particle. Figure 9 discloses that the behavior of the solutions boosts up for both the temperature distribution and as well as for the

concentration of nanoparticles for bigger values of  $Nt$ . Physically, diffusion enters into the fluid deeper by enhancing  $Nt$  which grounds to increase in concentration and thermal boundary layers. Further, the impact of  $Nt$  being further marked on the volume fraction contrast in temperature.

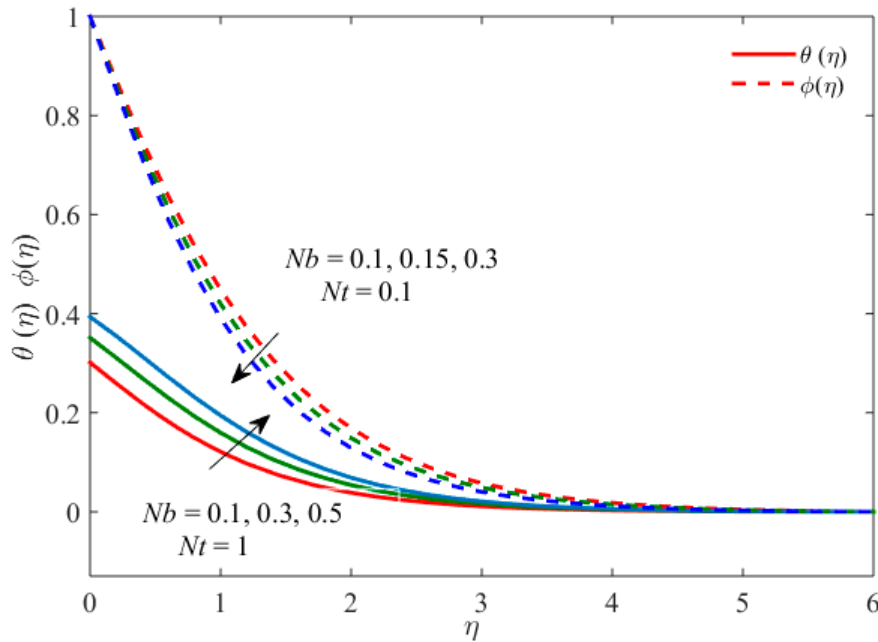


Figure 8. The influence of  $Nb$  on  $\theta(\eta)$ ,  $\phi(\eta)$ .

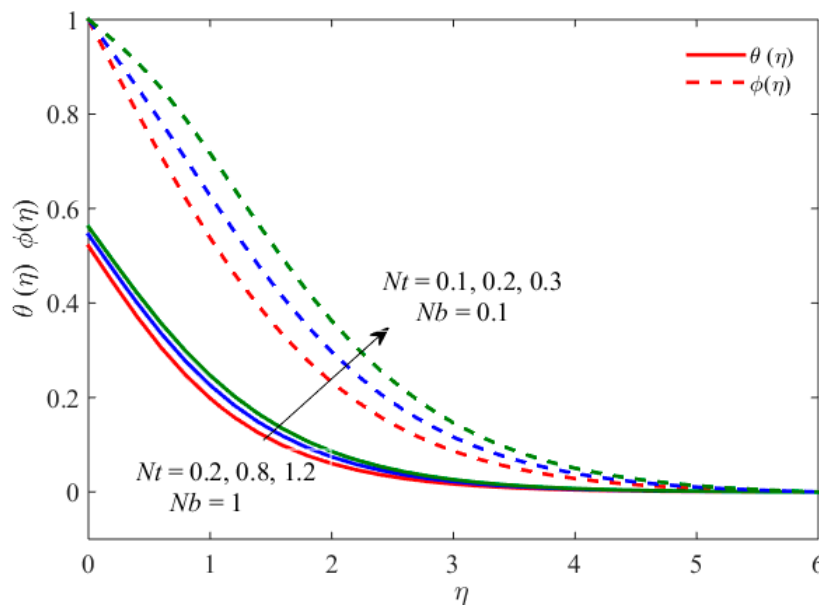


Figure 9. The influence of  $Nt$  on  $\theta(\eta)$ ,  $\phi(\eta)$ .

The outcome of convective parameter  $\gamma$  on  $\theta(\eta)$  and  $\phi(\eta)$  are portrayed in Figure 10. It is analyzed from these figures that the profiles of  $\theta(\eta)$  and  $\phi(\eta)$  elevated as  $\gamma$  raises. The strong convective heat at the sheet appearing due to mounting values of  $\gamma$ , which growing the temperature and concentration. It authorized the species and as well as the thermal effect to pierce deeper into the quiescent fluid. As a result of the outcome they augmented the boundary layer with widening  $\gamma$  for both the temperature and as well as the concentration. Figure 11 depicts the behavior of thermal relaxation constraint  $\tau$  on  $\theta(\eta)$ . The results indicate that the temperature of fluid declines with augmenting thermal relaxation

parameter. Physically, enhancing the thermal relaxation parameter increases the gap between the liquid molecules and due to these effects, the temperature of fluid depreciates.

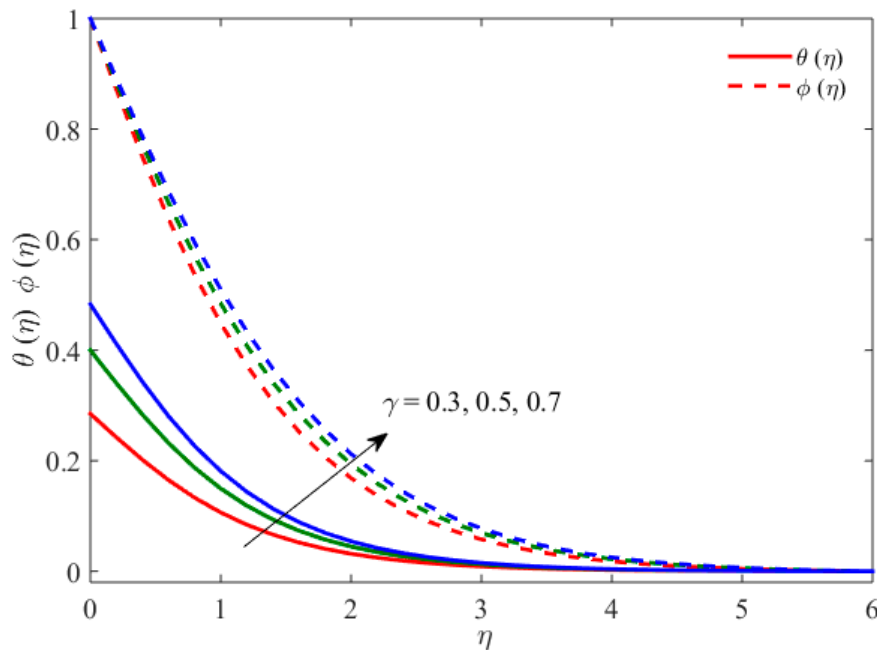


Figure 10. The influence of  $\gamma$  on  $\theta(\eta)$ ,  $\phi(\eta)$ .

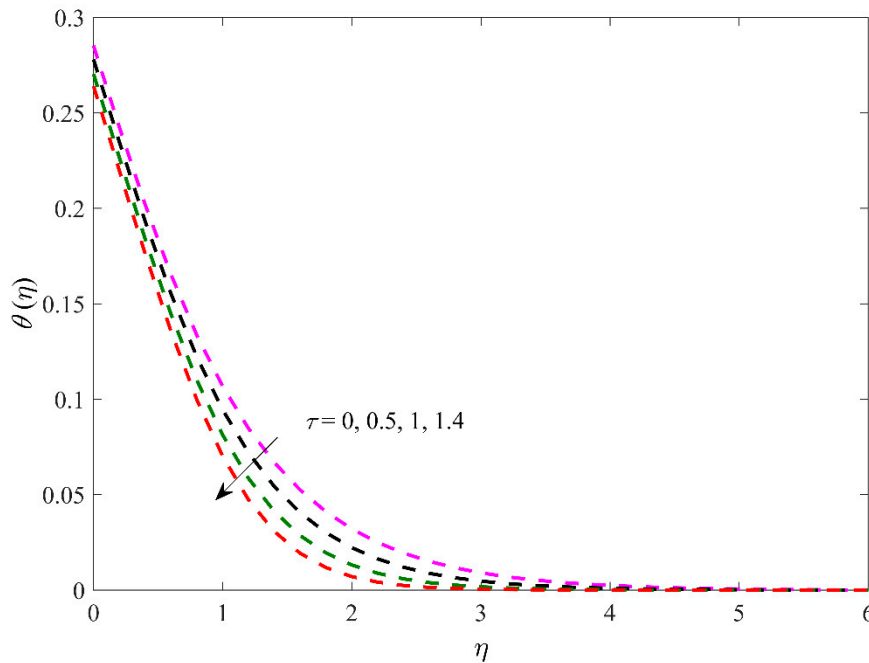


Figure 11. The influence of  $\tau$  on  $\theta(\eta)$ .

Figures 12–15 intricate the deviation of entropy generation for preferred values of aligned angle  $\zeta$ , Brinkman number  $Br$ , Reynolds number  $Re_L$  and magnetic parameter  $M$ . Figure 12 predicts that the profile of entropy generation decreases with growing  $\zeta$ . Figure 13 reveals that the entropy generation augments due to larger  $M$ . It perceives that the magnetic field is a resource of entropy generation to the heat transfer and friction of fluid. It can be finalized that the entropy generation can be controlled by taking a small magnetic parameter which is an important issue in the propulsion of MHD nuclear. It is perceived from Figures 14 and 15 that entropy profile accelerates by growing either  $Br$  or Reynolds

number. As the entropy generation created from machines of all irreversibility and consequently the entropy generation rises with augmenting  $Re_L$ . The higher amount in the entropy generation formed via the irreversibility of liquid friction happens owing to growing  $Br$ .

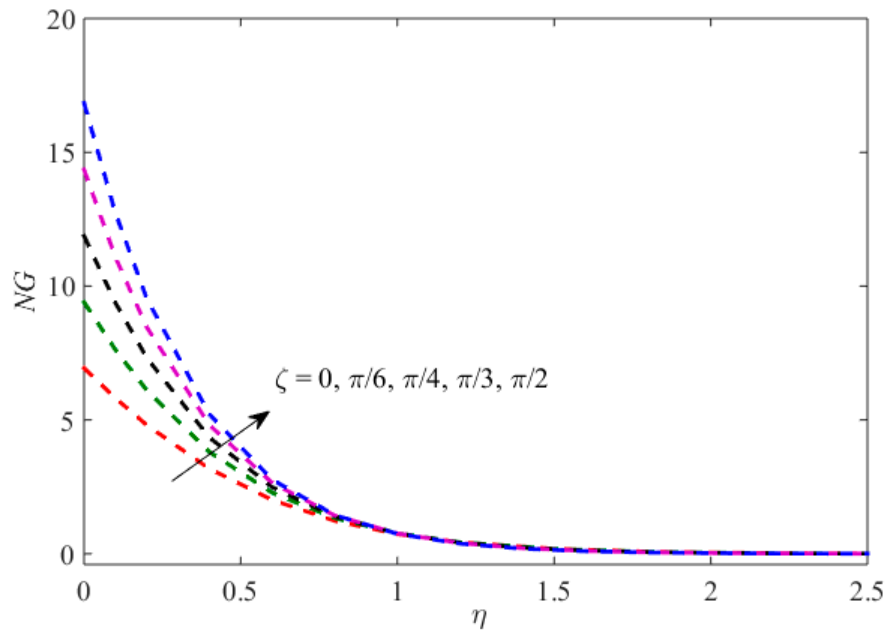


Figure 12. Entropy generation for  $\zeta$ .

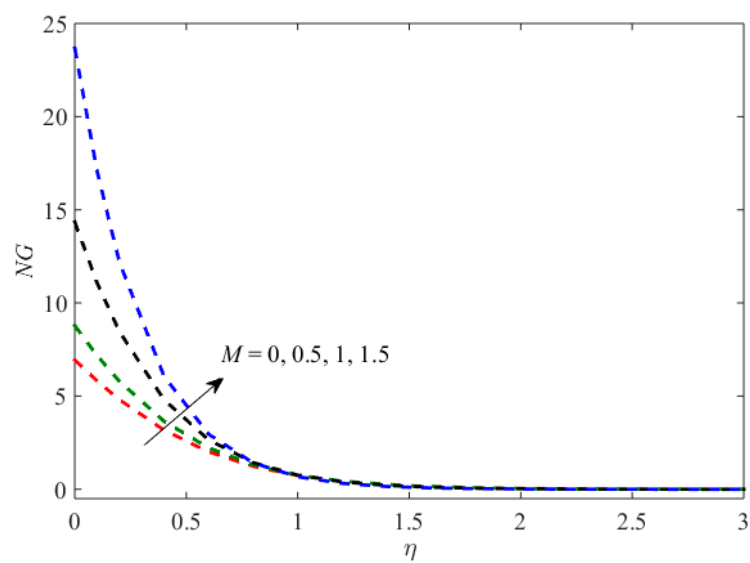


Figure 13. Entropy generation for  $M$ .

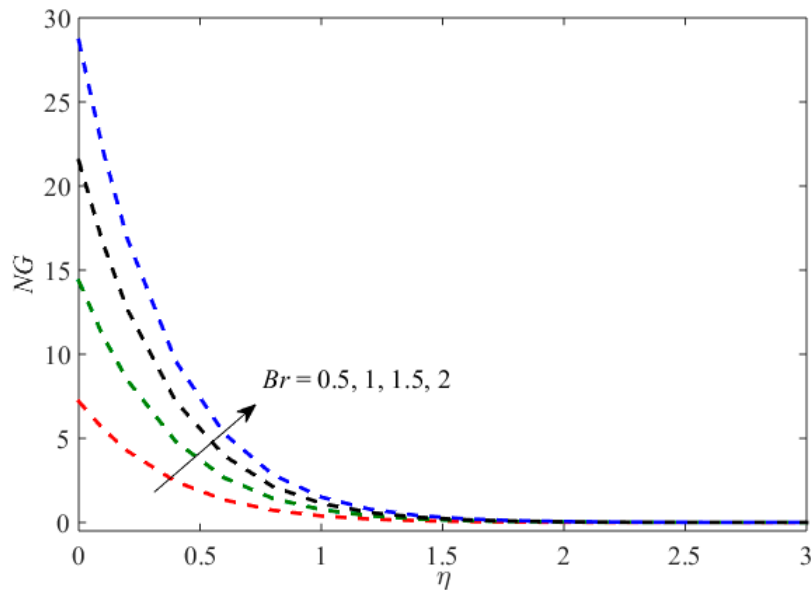


Figure 14. Entropy generation for  $Br$ .

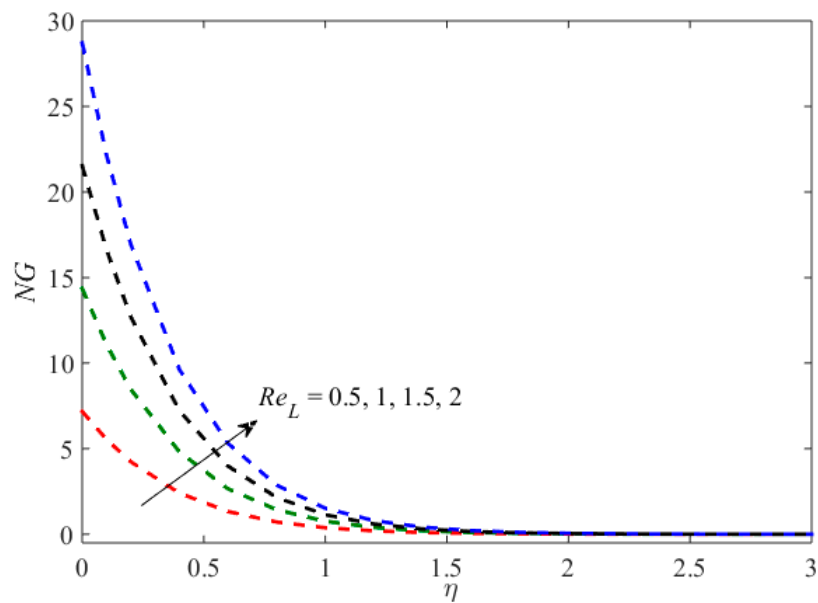
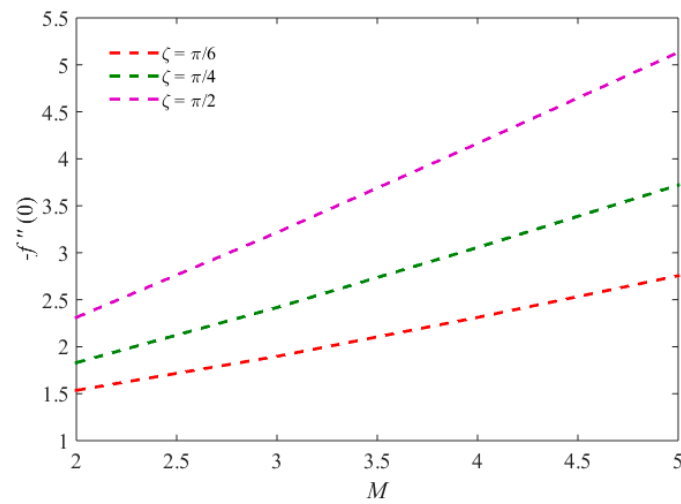
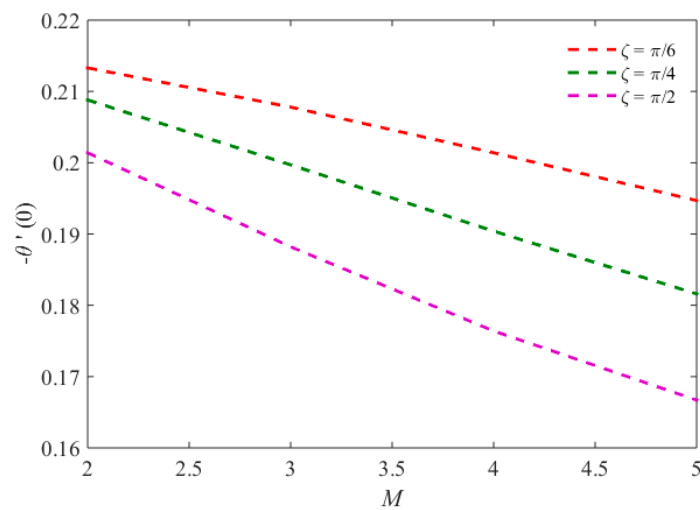


Figure 15. Entropy generation for  $Re_L$ .

The essential physical quantities  $-f''(0)$ ,  $-\theta'(0)$  and  $-\phi'(0)$  with  $M$  are discussed in Figures 16–18, respectively. Figure 16 reveals that the values of  $-f''(0)$  uplifts due to  $\zeta$ . It is also inspected that the values of  $-f''(0)$  significantly enhances as  $M$  enhances. Whereas, the values of  $-\theta'(0)$  and  $-\phi'(0)$  decay due to  $\zeta$  as shown in Figures 17 and 18, respectively, while these values appreciably decline with increasing values of  $M$ . These values are also tabulated in Table 2. Moreover, the values of  $-f''(0)$ ,  $-\theta'(0)$  and  $-\phi'(0)$  are positive, indicating that mass and heat species are mutated from the warm sheet to the cold liquid.



**Figure 16.** Influence of  $\zeta$  on  $-f'''(0)$  versus  $M$ .



**Figure 17.** Influence of  $\zeta$  on  $-\theta'(0)$  versus  $M$ .

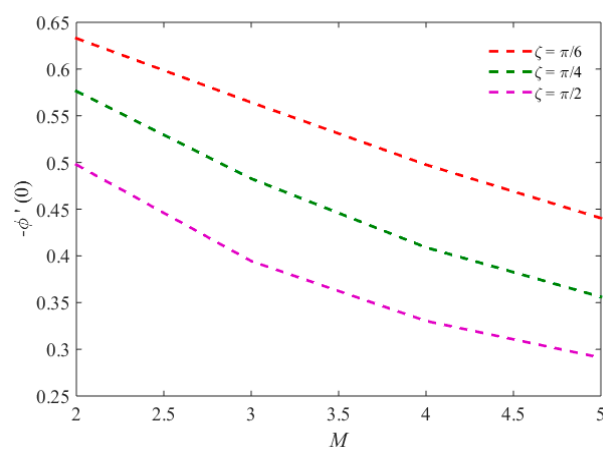


**Figure 18.** Influence of  $\zeta$  on  $-\phi'(0)$  versus  $M$ .

**Table 2.** Values of  $-f''(0)$ ,  $-\theta'(0)$  and  $-\phi'(0)$  versus  $M$  for different values of  $\zeta$  when  $Nb = 0.1, Nt = 0.1, \tau = 0.02, \gamma = 0.3, Pr = Sc = 1$  are fixed.

$M$	$\zeta$	$-f''(0)$	$-\theta'(0)$	$-\phi'(0)$
2	$\pi/6$	1.5357	0.2133	0.6329
	$\pi/4$	1.8305	0.2088	0.5763
	$\pi/2$	2.3117	0.2014	0.4976
3	$\pi/6$	1.8972	0.2078	0.5643
	$\pi/4$	2.4172	0.1997	0.4827
	$\pi/2$	3.2154	0.1882	0.3944
4	$\pi/6$	2.3117	0.2014	0.4976
	$\pi/4$	3.0560	0.1904	0.4090
	$\pi/2$	4.1637	0.1764	0.3303
5	$\pi/6$	2.7551	0.1947	0.4404
	$\pi/4$	3.7198	0.1816	0.3561
	$\pi/2$	5.1318	0.1667	0.2910

## 5. Final Remarks

The impacts of entropy generation and Cattaneo–Christov heat flux on MHD aligned flow past a radial convectively-heated stretched sheet comprising nanoparticles were studied numerically. The governing equations are developed into ODE's via the similar scaling transformation and these equations worked out numerically via the bvp4c solver. The subsequent attention-grabbing results can be ported from this research:

- The fluid flow velocity diminishes due to aligned angle, while the temperature and concentration of nanoparticles show escalating behavior.
- The velocity profile decays due to magnetic parameter, whereas concentration of nanoparticles and temperature display opposite behavior.
- The impacts of Brownian and thermophoresis parameter on temperature distribution are identical.
- The influences of motion of Brownian and thermophoresis on the volume fraction are opposite.
- Temperature distribution as well as the concentration of nanofluid improves due to convective parameter.
- Due to the thermal relaxation parameter, the temperature distribution declines.
- An entropy profile becomes larger for bigger values of aligned angle, Reynolds number, magnetic parameter, the Brinkman number.
- The values of  $-f''(0)$  appreciably increase due to aligned angle, while the values of  $-\theta'(0)$  and  $-\phi'(0)$  decay.

**Author Contributions:** Conceptualization, A.Z.; Formal analysis, A.Z. and U.K.; Investigation, U.K. Methodology, A.Z., I.K., A.H.S. and E.-S.M.S.; Project administration, A.Z., U.K. and I.K.; Software, I.K.

**Funding:** The authors would like to extend their sincere appreciation to the Deanship of Scientific Research at King Saud University for its funding of this research through the Research Group Project No. RGP-160.

**Conflicts of Interest:** The authors declare no conflict of interest.

## Nomenclature

$Be$	Bejan number
$\ddot{B}_0$	intensity of magnetic field
$Br$	Brinkman number
$c$	positive constant
$C_{fx}$	skin friction coefficient
$\ddot{C}$	concentration of nanoparticles
$\ddot{C}_\infty$	ambient concentration of nanoparticles
$\ddot{D}_B$	the Brownian constraint
$\ddot{D}_T$	the thermophoresis diffusion
$\ddot{h}_f$	heat transfer coefficient
$k$	thermal conductivity
$L$	characteristic length
$M$	magnetic parameter
$m_w$	mass flux
$Nb$	Brownian parameter
$NG$	volumetric rate of entropy generation
$Nt$	thermophoresis parameter
$Nu_x$	Nusselt number
$Pr$	Prandtl number
$q_w$	heat flux
$Re_r$	local Reynolds number
$Re_L$	the characteristic length based Reynolds number
$Sc$	Schmidt number
$S_{gen}'''$	generated entropy
$S_0$	entropy generation characteristic
$\ddot{T}$	temperature
$\ddot{T}_f$	temperature of the hot liquid
$\ddot{T}_\infty$	ambient temperature
$(\ddot{w}, \ddot{u})$	velocity components
$(\ddot{r}, \ddot{z})$	Cartesian coordinates

## Greek symbols

$\ddot{\alpha}$	thermal diffusivity
$\Gamma$	time relaxation of heat flux
$\gamma$	convective parameter
$\varsigma$	aligned acute angle
$\lambda$	diffusive constant
$\phi$	dimensionless concentration of nanoparticle
$\theta$	dimensionless temperature
$\ddot{\nu}$	kinematic viscosity
$\ddot{\rho}$	the density
$\ddot{\sigma}$	the electrical conductivity
$\tau$	thermal relaxation parameter
$\Omega$	capacity ratio
$\Omega_1$	temperature difference
$\ddot{\tau}_w$	shear stress
$\psi$	stream function
$\eta$	similarity variable

## Superscripts

'	derivative w.r.t. $\eta$
---	--------------------------

## References

1. Choi, S.U.S.; Eastman, J.A. Enhancing thermal conductivity of fluids with nanoparticles. *ASME Fluids Eng. Div.* **1995**, *231*, 99–105.
2. Buongiorno, J. Convective transport in nanofluids. *ASME J. Heat Transf.* **2006**, *128*, 240–250. [[CrossRef](#)]
3. Nield, D.A.; Kuznetsov, A.V. The Cheng–Minkowycz problem for natural convective boundary-layer flow in a porous medium saturated by a nanofluid. *Int. J. Heat Mass Transf.* **2009**, *52*, 5792–5795. [[CrossRef](#)]
4. Khan, W.A.; Pop, I. Boundary-layer flow of a nanofluid past a stretching sheet. *Int. J. Heat Mass Transf.* **2010**, *53*, 2477–2483. [[CrossRef](#)]
5. Turkyilmazoglu, M. Analytical solutions of single and multi-phase models for the condensation of nanofluid film flow and heat transfer. *Eur. J. Mech. B Fluids* **2015**, *53*, 272–277. [[CrossRef](#)]
6. Pour, M.S.; Nassab, S.A.G. Numerical investigation of forced laminar convection flow of nanofluids over a backward facing step under bleeding condition. *J. Mech.* **2012**, *28*, 7–12. [[CrossRef](#)]
7. Goodarzi, M.; Safaei, M.R.; Vafai, K.; Ahmadi, G.; Dahari, M.; Kazi, S.N.; Jomhari, N. Investigation of nanofluid mixed convection in a shallow cavity using a two-phase mixture model. *Int. J. Thermal Sci.* **2014**, *75*, 204–220. [[CrossRef](#)]
8. Mustafa, M.; Khan, J.A.; Hayat, T.; Alsaedi, A. Analytical and numerical solutions for axisymmetric flow of nanofluid due to non-linearly stretching sheet. *Int. J. Non Linear Mech.* **2015**, *71*, 22–29. [[CrossRef](#)]
9. Akbari, O.A.; Safaei, M.R.; Goodarzi, M.; Akbar, N.S.; Zarringhalam, M.; Ahmadi, G.; Shabani, S.; Dahari, M. A modified two-phase mixture model of nanofluid flow and heat transfer in a 3-D curved microtube. *Adv. Powder Technol.* **2016**, *27*, 2175–2185. [[CrossRef](#)]
10. Khan, M.; Azam, M. Unsteady heat and mass transfer mechanisms in MHD Carreau nanofluid flow. *J. Mol. Liq.* **2017**, *225*, 554–562. [[CrossRef](#)]
11. Hussanan, A.; Salleh, M.Z.; Khan, I. Microstructure and inertial characteristics of a magnetite ferrofluid over a stretching/shrinking sheet using effective thermal conductivity model. *J. Mol. Liq.* **2018**, *255*, 64–75. [[CrossRef](#)]
12. Rafique, K.; Anwar, M.I.; Misiran, M.; Khan, I.; Seikh, A.H.; Sharif, E.S.M.; Nisar, K.S. Brownian motion and thermophoretic diffusion effects on micropolar type nanofluid flow with Soret and Dufour impacts over an inclined sheet: Keller-box simulations. *Energies* **2019**, *12*, 4191. [[CrossRef](#)]
13. Yousefzadeh, S.; Rajabi, H.; Ghajari, N.; Sarafraz, M.M.; Akbari, O.A.; Goodarzi, M. Numerical investigation of mixed convection heat transfer behavior of nanofluid in a cavity with different heat transfer areas. *J. Thermal Anal. Calorim.* **2019**. [[CrossRef](#)]
14. Faraz, F.; Haider, S.; Imran, S.M. Study of magneto-hydrodynamics (MHD) impacts on an axisymmetric Casson nanofluid flow and heat transfer over unsteady radially stretching sheet. *SN Appl. Sci.* **2020**, *2*, 14. [[CrossRef](#)]
15. Bagherzadeh, S.A.; Jalali, E.; Sarafraz, M.M.; Akbari, O.A.; Karimipour, A.; Goodarzi, M.; Bach, Q.-V. Effects of magnetic field on micro cross jet injection of dispersed nanoparticles in a microchannel. *Int. J. Num. Meth. Heat Fluid Flow* **2019**. [[CrossRef](#)]
16. Tian, Z.; Etedali, S.; Afrand, M.; Abdollahi, A.; Goodarzi, M. Experimental study of the effect of various surfactants on surface sediment and pool boiling heat transfer coefficient of silica/DI water nano-fluid. *Powder Technol.* **2019**, *356*, 391–402. [[CrossRef](#)]
17. Spasojević, M.D.; Janković, M.R.; Djaković, D.D. A new approach to entropy production minimization in diabatic distillation column with trays. *Therm. Sci.* **2010**, *14*, 317–328. [[CrossRef](#)]
18. Abu-Nada, E. Investigation of entropy generation over a backward facing step under bleeding conditions. *Energy Convers. Manag.* **2008**, *49*, 3237–3242. [[CrossRef](#)]
19. Komurgoz, G.; Arikoglu, A.; Ozkol, I. Analysis of the magnetic effect on entropy generation in an inclined channel partially filled with porous medium. *Numer. Heat Transf. Part A Appl.* **2012**, *61*, 786–799. [[CrossRef](#)]
20. Butt, A.S.; Ali, A. Entropy effects in hydromagnetic free convection flow past a vertical plate embedded in a porous medium in the presence of thermal radiation. *Eur. Phys. J. Plus* **2013**, *128*, 51–55. [[CrossRef](#)]
21. Rashidi, M.M.; Kavyani, N.; Abelman, S. Investigation of entropy generation in MHD and slip flow over a rotating porous disk with variable properties. *Int. J. Heat Mass Transf.* **2014**, *70*, 892–917. [[CrossRef](#)]

22. Goodarzi, M.; Safaei, M.R.; Oztop, H.F.; Karimipour, A.; Sadeghinezhad, E.; Dahari, M.; Kazi, S.N.; Jomhari, N. Numerical study of entropy generation due to coupled laminar and turbulent mixed convection and thermal radiation in an enclosure filled with a semitransparent medium. *Sci. World J.* **2014**, *2014*, 1–8. [[CrossRef](#)] [[PubMed](#)]
23. Das, S.; Chakraborty, S.; Jana, R.N.; Makinde, O.D. Entropy analysis of unsteady magneto-nanofluid flow past accelerating stretching sheet with convective boundary condition. *Appl. Math. Mech.* **2015**, *36*, 1593–1610. [[CrossRef](#)]
24. Shateyi, S.; Motsa, S.S.; Makukula, Z. On spectral relaxation method for entropy generation on a MHD flow and heat transfer of a Maxwell fluid. *J. App. Fluid Mech.* **2015**, *8*, 21–31.
25. Rehman, S.U.; Haq, R.U.; Khan, Z.H.; Lee, C. Entropy generation analysis for non-Newtonian nanofluid with zero normal flux of nanoparticles at the stretching surface. *J. Taiwan Inst. Chem. Eng.* **2016**, *63*, 226–235. [[CrossRef](#)]
26. Almakki, M.; Dey, S.; Mondal, S.; Sibanda, P. On unsteady three-dimensional axisymmetric MHD nanofluid flow with entropy generation and thermo-diffusion effects on a non-linear stretching sheet. *Entropy* **2017**, *19*, 168. [[CrossRef](#)]
27. Afridi, M.I.; Qasim, M.; Khan, I. Entropy generation minimization in MHD boundary layer flow over a slendering stretching sheet in the presence of frictional and Joule heating. *J. Korean Phys. Soc.* **2018**, *73*, 1303–1309. [[CrossRef](#)]
28. Hayat, T.; Khan, M.W.A.; Khan, M.I.; Alsaedi, A. Nonlinear radiative heat flux and heat source/sink on entropy generation minimization rate. *Phys. B Phys. Cond. Matt.* **2018**, *538*, 95–103. [[CrossRef](#)]
29. Aghaei, A.; Sheikhzadeh, G.A.; Goodarzi, M.; Hasani, H.; Damirchi, H.; Afrand, M. Effect of horizontal and vertical elliptic baffles inside an enclosure on the mixed convection of a MWCNTs-water nanofluid and its entropy generation. *Eur. Phys. J. Plus* **2018**, *133*, 486. [[CrossRef](#)]
30. El-Aziz, M.A.; Afify, A.A. MHD Casson fluid flow over a stretching sheet with entropy generation analysis and Hall influence. *Entropy* **2019**, *21*, 592. [[CrossRef](#)]
31. Pordanjani, A.H.; Aghakhani, S.; Karimipour, A.; Afrand, M.; Goodarzi, M. Investigation of free convection heat transfer and entropy generation of nanofluid flow inside a cavity affected by magnetic field and thermal radiation. *J. Thermal Anal. Calorim.* **2019**, *137*, 997–1019. [[CrossRef](#)]
32. Cattaneo, C. Sulla conduzionedelcalore. *Atti Semin. Mat. Fis. Univ. Modena Reggio Emilia* **1948**, *3*, 83–101.
33. Christov, C.I. On frame indifferent formulation of the Maxwell-Cattaneo model of finite speed heat conduction. *Mech. Res. Commun.* **2009**, *36*, 481–486. [[CrossRef](#)]
34. Straughan, B. Thermal convection with the Cattaneo-Christov model. *Int. J. Heat Mass Transf.* **2010**, *53*, 95–98. [[CrossRef](#)]
35. Li, J.; Zheng, L.; Liu, I. MHD viscoelastic flow and heat transfer over a vertical stretching sheet with Cattaneo-Christov heat flux effects. *J. Mol. Liq.* **2016**, *221*, 19–25. [[CrossRef](#)]
36. Ramzan, M.; Bilal, M.; Chung, J.D. Effects of MHD homogeneous-heterogeneous reactions on third grade fluid flow with Cattaneo-Christov heat flux. *J. Mol. Liq.* **2016**, *223*, 1284–1290. [[CrossRef](#)]
37. Hayat; Khan, M. On Cattaneo-Christov heat flux model for Carreau fluid flow over a slendering sheet. *Resul. Phys.* **2017**, *7*, 310–319. [[CrossRef](#)]
38. Hayat, T.; Khan, M.I.; Farooq, M.; Alsaedi, A.; Khan, M.I. Thermally stratified stretching flow with Cattaneo-Christov heat flux. *Int. J. Heat Mass Transf.* **2017**, *106*, 289–294. [[CrossRef](#)]
39. Ali, M.E.; Sandeep, N. Cattaneo-Christov model for radiative heat transfer of magnetohydrodynamic Casson-ferrofluid: A numerical study. *Results Phys.* **2017**, *7*, 21–30. [[CrossRef](#)]
40. Babu, M.J.; Sandeep, N.; Saleem, S. Free convective MHD Cattaneo-Christov flow over three different geometries with thermophoresis and Brownian motion. *Alex. Eng. J.* **2017**, *56*, 659–669. [[CrossRef](#)]
41. Mahanthesh, B.; Gireesha, B.J.; Raju, C.S.K. Cattaneo-Christov heat flux on UCM nanofluid flow across a melting surface with double stratification and exponential space dependent internal heat source. *Inform. Med. Unlock.* **2017**, *9*, 26–34. [[CrossRef](#)]

42. Butt, A.S.; Ali, A. Entropy analysis of magnetohydrodynamic flow and heat transfer over a convectively heated radially stretching surface. *J. Taiwan Inst. Chem. Eng.* **2014**, *45*, 1197–1203. [[CrossRef](#)]
43. Soid, S.K.; Ishak, A. MHD flow and heat transfer over a radially stretching/shrinking disk. *Chin. J. Phys.* **2018**, *56*, 58–66. [[CrossRef](#)]



© 2019 by the authors. Licensee MDPI, Basel, Switzerland. This article is an open access article distributed under the terms and conditions of the Creative Commons Attribution (CC BY) license (<http://creativecommons.org/licenses/by/4.0/>).